

Banding in Entangled Polymer Fluids under Oscillatory Shearing

Prashant Tapadia, Sham Ravindranath, and Shi-Qing Wang*

Department of Polymer Science, University of Akron, Akron, Ohio 44325, USA

(Received 12 December 2005; published 16 May 2006)

We report a flow phenomenon in entangled polymer solutions that has never been described in the literature. A large-amplitude oscillatory shear was imposed on the polymer sample at a frequency higher than the overall chain relaxation rate. The resulting chain orientation led to a new environment in which the initially well-entangled chains managed to disentangle inhomogeneously in space. A layer lacking chain entanglement developed to take the load of the imposed strain. As a result of this nonlinearity, the rest of the sample avoided significant deformation and its chain entanglement remained intact.

DOI: [10.1103/PhysRevLett.96.196001](https://doi.org/10.1103/PhysRevLett.96.196001)

PACS numbers: 83.10.Gr, 83.60.Df, 83.80.Sg

Liquids that possess a linear relationship between shear stress σ and shear rate $\dot{\gamma}$ are known as Newtonian fluids, where the proportionality constant is viscosity η . Polymeric liquids, made of long linear chains that form entanglement since they cannot pass over one another without breaking, are an important class of non-Newtonian fluids, whose viscosity η takes a finite time to reach the steady state value and decreases with $\dot{\gamma}$. This widely known shear thinning behavior was thought to occur gradually due to increased chain alignment in shear that leads to disentanglement. If the chain disentanglement event was not to occur catastrophically in shear flow as agreed upon by the current consensus, shear thinning would take place homogeneously in every layer across the sample thickness. Then, just as in the case of Newtonian fluids, imposition of V on one surface over the other stationary surface in a parallel-plate device of gap H would indeed result in a homogeneous flow with shear rate V/H prevailing in every layer.

Many structured materials, such as micellar solutions [1,2], dense suspensions [3], foams [4,5], liquid crystals [6], soft gels and glasses [7], granular fluids, and metals [8–10], respond to large external deformation catastrophically: The imposed shear deformation or rate of deformation can produce a spatially nonhomogeneous distribution of different states across the sample thickness. This is commonly known as shear banding [11]. Entangled model polymer solutions have also recently been found to show a spatial variation in the shear rate measured across the sample thickness in startup shear [12]. This finding makes it rather difficult to establish a constitutive relationship between σ and $\dot{\gamma}$ through rheological measurements. It also challenges the currently favored version of the theoretical description [13] of entangled polymers in shear flow that arose from a decade of theoretical efforts [14–16] based on the de Gennes' visualization of snakelike motion of a test chain [17] within the Edwards' tube picture [18]. Furthermore, it calls for an reexamination of previous experimental studies of similar entangled polymer solutions [19–21].

Inspired by the previous results on continuous shear behavior of entangled polymer solutions, we have carried out further experiments in the present work to decipher how chains actually negotiate with one another to establish any new topological relationship during shear. Specifically, in this work, we apply large-amplitude oscillatory shear (LAOS) to illustrate some intriguing flow behavior of entangled liquids by using an effective particle-tracking velocimetric method to determine the velocity profile in LAOS. The results indicate that chain disentanglement, as the cause of shear thinning, also occurs inhomogeneously in space in LAOS.

The entangled polymer solutions under examination are a previously prepared and studied 10 wt.% 1,4-polybutadiene (PBD) solution [22], made of a high weight PBD of $M_w = 1.2 \times 10^6$ g/mol and $M_w/M_n = 1.18$ from Polymer Source, Inc., dissolved in a phenyl-terminated oligomeric butadiene (oBD) of $M_n = 1.0$ kg/mol (Aldrich 20041-7), and a newly made 10% PBD solution of a monodisperse PBD of $M_w = 740$ kg/mol (made at Bridgestone) in a monodisperse oBD of $M_w = 4$ kg/mol (made at Goodyear). For the particle-tracking purpose, the sample was seeded with silver-coated particles of 10 μ m diameter (Dantec Dynamics HGS-10) at a level of several hundred parts per million. A strain-controlled shear rheometer equipped with a cone-plate assembly of 25 mm diameter was employed in this study.

Our particle-tracking velocimetry, as illustrated in Fig. 1, consists of sending a laser beam either along the velocity gradient direction or at an angle to the shearing surface and videotaping the illuminated moving particles with a black-white CCD camera (with minimum 0.3 lx and maximum 30 frames per second) that is mounted with a DIN objective ($3.2 \times$) through an adaptive tube (Edmund Optics: U54-868). In scheme A, a transparent film surrounds the meniscus to allow focus of a telemicro lens onto the interior. The perturbation of the confining film on the simple shear flow inside the cone-plate cell can be evaluated and is removable by employing scheme B. In the present work, scheme A was set up for an advanced rheo-

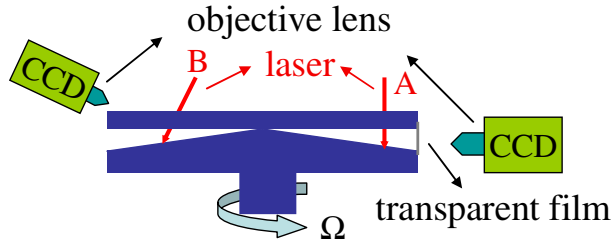


FIG. 1 (color online). The two setups of the particle-tracking velocimetry, where the upper stationary plate is made of transparent glass, the lower rotating cone made of steel, and $\theta = 5^\circ$. With laser A, the CCD camera is placed horizontally, watching the illuminating particles through a transparent film wrapped around the meniscus; with laser B, the camera is placed to look through the transparent upper shearing plate without any film around the meniscus.

metrics expansion system, where a bottom cone rotates against a fixed upper plate; scheme B was set up for a Bohlin CVOR rheometer (Malvern Instruments) where an upper cone rotates. Results from both protocols will be presented below.

Let us consider oscillatory shear by sandwiching a sample between cone and plate as shown in Fig. 1, where the cone would make an oscillatory torsional motion against the fixed plate, as described by angular displacement $\phi(t) = \phi_0 \sin \omega t$ and velocity by $\Omega = \phi_0 \omega \cos \omega t$. The shear strain is usually taken to be *uniform* across the gap equal to $\gamma_0 = X_0(r)/h(r) \cong \phi_0/\theta$, with $X_0(r) = \phi_0 r$, where $h(r) = r \tan \theta \cong r\theta$ is the gap distance at r . At low amplitudes $\gamma_0 \ll 1$, the storage modulus G' and loss modulus G'' were obtained as a function of ω , indicating that the overall chain relaxation rate, i.e., the crossover frequency ω_c (at which $G' = G''$), was around 0.07 rad/s for the entangled liquid. When the oscillatory shear was applied at frequencies $\omega > \omega_c$, the entangled chains would tend to deform and orient affinely without being able to relax significantly during the shear reversal in each cycle.

We subjected the sample to LAOS for a sufficiently long time at $\omega = 1 \text{ rad/s} > \omega_c$ to illustrate the effect of LAOS on the molecular reorganization. In the first cycle, the shear deformation was uniform across the gap, and such a uniform deformation also prevailed for $\gamma_0 \leq 1$ even at long times. But, over time, something dramatic took place. One key result of our particle-tracking velocimetric measurements is shown in Fig. 2. As one way to visualize the effect of LAOS, we analyzed the velocity field at the instant of the maximum Ω of the rotating cone. The video recording can also be analyzed at any other moments during each cycle. The measurements typically involve playing the movie frame by frame at a fixed rate of 30 frames per second using MGI VIDEOWAVE 4 software for about one to three frames and measuring, on a computer monitor, the displacement of the traced particles over these frames in the

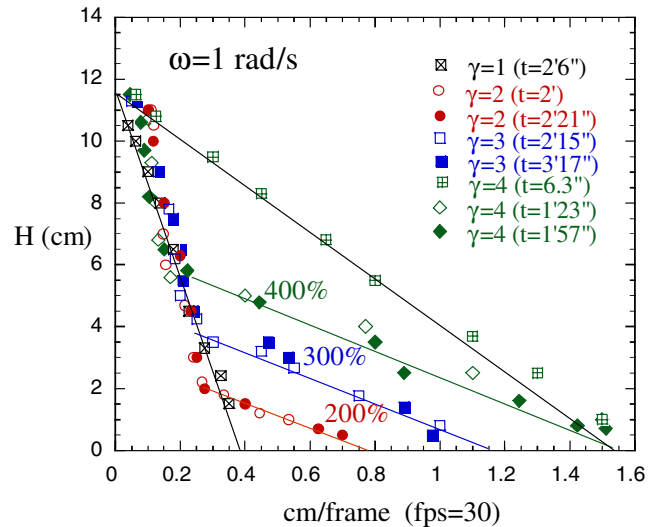


FIG. 2 (color online). The velocity profiles, evaluated from video observations based on scheme A in Fig. 1, of the well-entangled 10% PBD solution under oscillatory shear of four different strain amplitudes from 100% to 400%, all measured at the peak of the imposed angular velocities in the steady state (at the approximate different times indicated by the numbers in the parentheses) except for the plus-filled squares that represent the initial response of the sample 6.3 seconds after the start of the LAOS.

different layers across the sample thickness. The time resolution is therefore as good as about 0.1 s. In contrast to the linear velocity profile seen for $\gamma_0 = 1$ and at the beginning for $\gamma_0 = 4$, the steady state velocity profiles are highly nonlinear. The actual gap distance H was ca. 0.9 mm (i.e., about 10 mm from the cone center) and was 12 cm on the video display, where the measurements were taken and presented in Fig. 2. The reader can access a movie [23] showing the evolution of velocity profile for $\gamma_0 = 3$, based on which the open and solid squares were obtained in Fig. 2.

To remove the potential complications introduced by the confining film around the meniscus, we examine the velocity profile at LAOS of a different 10% PBD solution using a second rheometer from Malvern Instruments where an upper cone rotates against a fixed lower plate. Using scheme B as depicted in Fig. 1, we obtained another set of velocity profiles as shown in Fig. 3. The banding behavior is very similar to that shown in Fig. 2, and the difference arises from the difference in the makeup of these two different samples. Thus, this result indicates that there is a negligible effect at the location of observation from the stationary film surrounding the meniscus in scheme A in Fig. 1. To rule out the possibility that the observed banding would be due to a tiny stress gradient in the cone-plate setup, similar experiments have been conducted using parallel-disk shear cells, and the banding was also systematically observed [24].

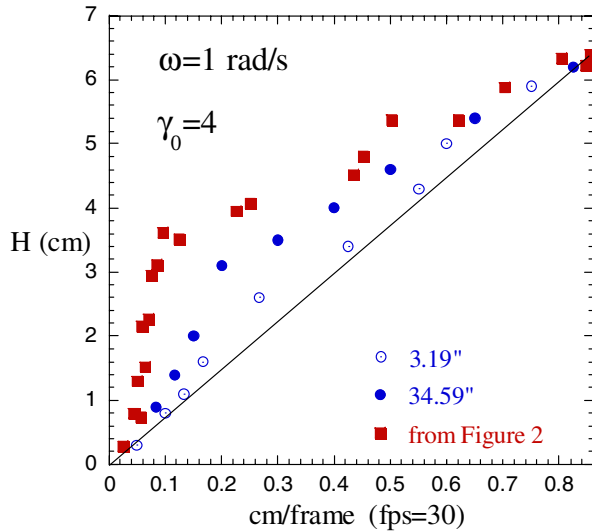


FIG. 3 (color online). The peak velocity profiles, which were measured based on scheme B in Fig. 1, of a different 10% PBD solution under LAOS of 400% where the data in Fig. 2 are also presented for comparison after rescaling the length scales, as well as the initial profile after half a cycle of oscillation.

Returning to Fig. 2, we note the banding characteristics to depend on the amplitude of the imposed strain. The peak shear rate $\dot{\gamma}_0 = \omega \gamma_0$ in the “fluid” layer reached 7.2 s^{-1} , whereas the “solid” top layer experienced a peak shear rate nearly tenfold smaller. In other words, the bottom layer experienced a shear strain as high as over 700%, whereas the top layer remained intact and was only undergoing deformation no greater than 100%. Upon increasing γ_0 from 2 to 4, the fractional thickness f of the fluid layer increased from $1/6$ to $1/2$, which can be described by $f = (\gamma_0 - 1)/6$, implying that no part of the sample would transform to a “fluid,” i.e., $f = 0$ when $\gamma_0 \leq 1$, which is indeed the case as shown in Fig. 2.

To elucidate the dynamics of this striking phenomenon, we followed the evolution (i.e., the thickness growth) of the disentangled layer over time. The flow behavior of the fluidlike layer looks distinctly different from that of the solidlike layer according to the visual impression of the recorded video. We can simply watch how the bottom layer grows in time and stop the video play to determine its thickness at the different time intervals. We first look for any amplitude effect at a fixed oscillation frequency of $\omega = 1 \text{ rad/s}$. Figure 4(a) shows that the sample reached its final state during the same time interval (ca. 100 s) regardless of the value of $\gamma_0 > 1$.

We next subjected the sample to an amplitude of $\gamma_0 = 3$ at various oscillation frequencies that were all higher than the chain relaxation rate of $\omega_c = 0.07 \text{ rad/s}$. Independent of the oscillation frequency ω , the final thicknesses of the fluid layer all attained 4 cm on the video monitor, or ca. $1/3$ of the total sample thickness, at approximately the same time, around 100 s as shown in Fig. 4(b). Since ω differed

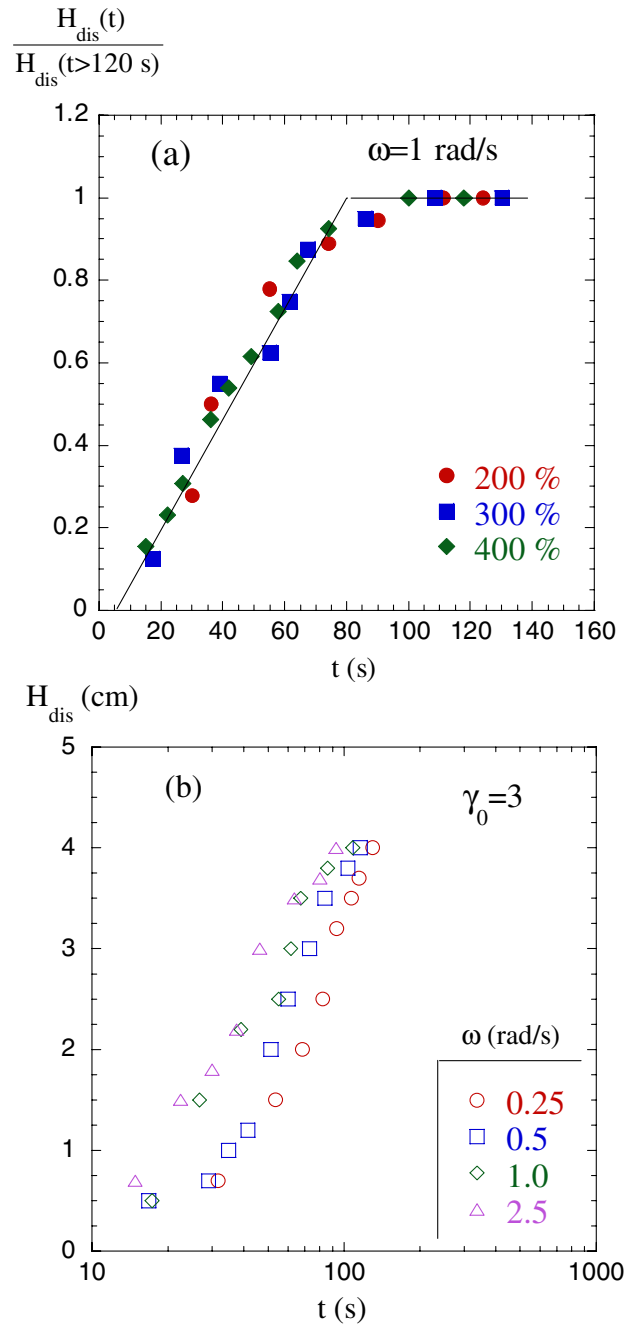


FIG. 4 (color online). The fluid layer thickness as a function of time based on the same video that produces Fig. 2: (a) normalized to show the kinetics of the layer growth at $\omega = 1 \text{ rad/s}$ for the different strain amplitudes and (b) for a strain amplitude of 300% at different oscillation frequencies.

by a factor of 10, in a given duration the sample had been subjected to 10 times as many cycles at $\omega = 25 \text{ rad/s}$ as it had at $\omega = 0.25 \text{ rad/s}$. Conversely, the total amount of cumulative shear strain γ_t was 10 times smaller at 0.25 than at 2.5 rad/s. Figure 4(b) shows that the growth time was hardly dependent on γ_t and ω and depended only on the time during which the sample was subjected to the LAOS

at $\omega > \omega_c$, indicating that flow convection played a minor role at most. Figure 4(a) further indicates that, as long as the strain amplitude was high enough (i.e., $\gamma_0 > 1$) to produce sufficient chain orientation, the kinetics leading to the final state were essentially the same, independent of γ_0 . This behavior is true only for the present highly polydisperse sample. Monodisperse samples display a different set of phenomena [24].

The preceding experimental observations indicate that the entangled solution is capable of rearranging over time into different states of entanglement in the various layers in simple shear. Specifically, the LAOS produced over time a coexistence of two different states of chain entanglement, indicating that the sample could not undergo chain disentanglement and shear thinning *uniformly* across the sample thickness. The key controlling variable appears to be a sufficiently high level of chain orientation as determined by the amplitude of the oscillatory shear. As long as the oscillation frequency is higher than the chain relaxation rate so that the imposed LAOS is effective to produce long-lasting chain orientation, the initially well-entangled chains find themselves in a new, anisotropic environment that allows them to look for a different topological relationship. With sufficient chain orientation, the chains seem to clear out of each other's way and enter a new dynamic state of less mutual constraint in a spatially inhomogeneous fashion, where some layers absorb the imposed strain by transforming into a state of disentanglement, allowing the rest of the sample to stay in a nearly equilibrium state of entanglement. The movie shows [23] that it actually took roughly only one period or a few seconds for the fluid layer to become visible, whereas the time required for the transformed layer to grow to its final thickness is much longer. The kinetics governing the growth was found to be insensitive to both ω and γ_0 . Currently, there is no theoretical description available to account for the nucleation and growth of the disentangled state in shear oscillation. However, let us hope that the available theoretical framework [25] can provide an adequate description of the reported phenomena.

In summary, the entangled polymer solution was found to respond to strain-controlled large-amplitude oscillatory shear by transforming partially into a state of lower viscosity and, thus, a lower level of chain entanglement. The response appears to show a state of frustration because the transformation (i.e., chain disentanglement) could not take place homogeneously as shown in Figs. 2 and 3. The coexistence of two layers of different viscoelastic properties under a given LAOS shows that chain disentanglement nucleates unevenly in space, taking place only under the critical condition of sufficient chain orientation. Here the "nucleation" appears to occur through chain diffusion as evidenced by the observations in Figs. 4(a) and 4(b). Ongoing work in our lab has shown other banding features

that are not observed here for the present rather polydisperse solutions [24]. Future reports will focus on the other mechanism responsible for shear banding in LAOS.

This work is supported, in part, by an ACS-PRF grant and an NSF grant.

*Corresponding author.

Electronic address: swang@uakron.edu

- [1] J.-B. Salmon, A. Colin, S. Manneville, and F. Molino, *Phys. Rev. Lett.* **90**, 228303 (2003).
- [2] O. Radulescu, P.D. Olmsted, J.P. Decruppe, S. Lerouge, J.F. Berret, and G. Porte, *Europhys. Lett.* **62**, 230 (2003).
- [3] W.M. Holmes, P.T. Callaghan, D. Vlassopoulos, and J. Roovers, *J. Rheol. (N.Y.)* **48**, 1085 (2004).
- [4] A. Kabla and G. Debregeas, *Phys. Rev. Lett.* **90**, 258303 (2003).
- [5] F. Rouyer, S. Cohen-Addad, and R. Hohler, *Colloids Surf. A* **263**, 111 (2005).
- [6] J.-B. Salmon, S. Manneville, and A. Colin, *Phys. Rev. E* **68**, 051503 (2003).
- [7] F. Varnik, L. Bocquet, and J.-L. Barrat, *J. Chem. Phys.* **120**, 2788 (2004).
- [8] A. Yu. Vinogradov and V.A. Khonik, *Philos. Mag.* **84**, 2147 (2004).
- [9] A.L. Greer, A. Castellero, S.V. Madge, I.T. Walker, and J.R. Wilde, *Mater. Sci. Eng. A* **375**, 1182 (2004).
- [10] A. Zaoui *et al.*, *Diffus. Defect Data, Solid State Data B, Solid State Phenom.* **B3-4**, 433 (1988).
- [11] C. Y.D. Lu, P.D. Olmsted, and R. C. Ball, *Phys. Rev. Lett.* **84**, 642 (2000).
- [12] P. Tapadia and S. Q. Wang, *Phys. Rev. Lett.* **96**, 016001 (2006).
- [13] R. S. Graham, A. E. Likhtman, T. C. B. McLeish, and S. T. Milner, *J. Rheol. (N.Y.)* **47**, 1171 (2003), and references therein. The reader is referred to this paper for a thorough review of the current theoretical status.
- [14] G. Marrucci, *J. Non-Newtonian Fluid Mech.* **62**, 279 (1996).
- [15] D.W. Mead, R. G. Larson, and M. Doi, *Macromolecules* **31**, 7895 (1998).
- [16] J. Bent *et al.*, *Science* **301**, 1691 (2003).
- [17] P. G. de Gennes, *J. Chem. Phys.* **55**, 572 (1971).
- [18] S.F. Edwards, *Proc. Phys. Soc. London* **92**, 9 (1967).
- [19] E. V. Menezes and W. W. Graessley, *J. Polym. Sci., Polym. Phys. Ed.* **20**, 1817 (1982).
- [20] M. Bercea, C. Peiti, B. Simionescu, and P. Navard, *Macromolecules* **26**, 7095 (1993).
- [21] C. Pattamaprom and R. G. Larson, *Macromolecules* **34**, 5229 (2001).
- [22] P. Tapadia and S. Q. Wang, *Phys. Rev. Lett.* **91**, 198301 (2003); *Macromolecules* **37**, 9083 (2004).
- [23] For the time-dependent velocity profile at $\omega = 1$ rad/s and $\gamma_0 = 3$, click Movie 3 at URL: <http://www3.uakron.edu/rheology/>.
- [24] S. Ravindranath and S. Q. Wang (to be published).
- [25] A. E. Likhtman, S. T. Milner, and T. C. B. McLeish, *Phys. Rev. Lett.* **85**, 4550 (2000).